Performance of MODFET and MESFET: A Comparative Study Including Equivalent Circuits Using Combined Electromagnetic and Solid-State Simulator

S. M. Sohel Imtiaz, *Member, IEEE,* and Samir M. El-Ghazaly, *Senior Member, IEEE*

***Abstract*—A combined electromagnetic and solid-state (CESS) simulation model for the analysis of submicrometer semiconductor devices including the electromagnetic-wave propagation effects is presented. The performance comparison of two important high-frequency devices—modulation doped field-effect transistor (MODFET) and metal–semiconductor field-effect transistor (MESFET)—are illustrated using this model. The CESS simulator couples a semiconductor model to the three-dimensional (3-D) time-domain solution of Maxwell's equations. The semiconductor model is based on the moments of the Boltzmann's transport equation. The simulation uses the electromagnetic-wave concept to emphasize the better performance of MODFET over MESFET. The electromagnetic-wave propagation effects on the two devices are thoroughly analyzed. The use of the electromagnetic model over the conventional quasi-static model provides the actual device response along the gatewidth at high frequencies. The exchange of energy between the electrons and the electromagnetic wave is observed. The CESS model also facilitates the optimum choice of the device width in terms of the output voltage. This model is capable of predicting the large-signal behavior of the submicrometer devices as well. The equivalent-circuit parameters are extracted at high frequencies for MODFET and MESFET, using a time-domain approach as well as a quasi-static approach.**

***Index Terms*—Device simulation, electromagnetics, MESFET's, MODFET's, semiconductor devices.**

NOMENCLATURE

$\boldsymbol{J}$	Current density.
n	Electron density.
q	Electronic charge.
t	Time.
$\boldsymbol{v}$	Electron velocity.
$v_{\rm ds}$	Drain-to-source voltage.
$v_{\rm gs}$	Gate-to-source voltage.
$i_{\rm ds}$	Drain-to-source current.
$i_{\rm gs}$	Gate current.
Q_g	Gate charge.
Q_d	Drain charge.
ω	Angular frequency.
g_m	Transconductance.
R_i	Gate-to-source resistance.
$C_{\rm gs}$	Gate-to-source capacitance.
$C_{\rm gd}$	Feedback capacitance.
$C_{\rm ds}$	Drain-to-source capacitance.
g_d	Drain conductance.
Y_{gg}	Gate admittance.
$Y_{\rm gd}$	Gate-to-drain admittance.
$Y_{\rm dg}$	Drain-to-gate admittance.
$Y_{\rm dd}$	Drain admittance.

Manuscript received February 5, 1997; revised April 7, 1998. This work was supported by the U.S. Army Research Office under Contract DAAH04-95-1-0252.

S. M. Sohel Imtiaz was with the Department of Electrical Engineering, Telecommunications Research Center, Arizona State University, Tempe, AZ 85287 USA. He is now with Micro Linear Corporation, San Jose, CA 95131 USA (e-mail: imtiazs@engmail.ulinear.com).

S. M. El-Ghazaly is with the Department of Electrical Engineering, Telecommunications Research Center, Arizona State University (ASU), Tempe, AZ 85287-7206 USA (e-mail: sme@asu.edu).

Publisher Item Identifier S 0018-9480(98)04960-6.

I. INTRODUCTION

THE modeling and simulation of semiconductor devices were previously achieved by solving various combinations of Poisson's equation, continuity equation, and the momentum and energy balance equations, in many different forms [1]–[11]. In most cases, the dc and low-frequency performances of semiconductor devices were analyzed. They are modified later for high-frequency simulation purposes. Moreover, these models are mostly in two dimensions, which do not include the electromagnetic-wave propagation effects. When the device operates in the millimeter-wave range, where the device width is comparable to the electromagnetic wavelength and the short wave period may be comparable to the electron relaxation times, the interactions of the conducting electrons with the electromagnetic wave cannot be neglected. In this paper, Maxwell's equations are used in conjunction with a three-dimensional (3-D) hydrodynamic model to develop a combined electromagnetic and solid-state (CESS) simulator for high-frequency devices, using the finite-difference time-domain (FDTD) method. When an ac signal is applied at the device input with appropriate dc bias, the CESS simulator predicts the correct device response and accounts for the energy transfer between the electrons and the electromagnetic wave.

The CESS model has a lot of potentials in characterizing the high-frequency semiconductor devices over the conventional

quasi-static model. It is capable of showing the transfer of energy between the device and the electromagnetic wave. Nonlinearity of the devices are evident in the responses obtained from the solution of the electromagnetic model while the quasi-static model shows linear behavior along the device width. The main advantage is achieved from this model in the solution of integrated circuits. Until now, the microwave amplifiers or any other integrated device structures are simulated in parts and the active devices are replaced by the lumped elements. This process loses a lot of information about the device, including the nonlinearity. The CESS model allows the direct coupling and integration of semiconductor devices [12]. In this method, all the device characteristics are preserved. This is a potential contribution of this model in high-frequency device simulations. The CESS model has already been proven to be a very powerful tool for analyzing the behavior of submicrometer gate MESFET's [13].

The microwave and millimeter-wave amplification of two important semiconductor devices [such as modulation doped field-effect transistor (MODFET) and metal–semiconductor field-effect transistor (MESFET)] created considerable excitement and optimism among the device as well as circuit engineers. A unified charge–control and carrier velocity–saturation model is used to compare the high-frequency performance of MODFET and MESFET in [14]. The model achieved useful power gains at high frequencies with reduced gate length. The dependence of carrier mobility, noise figure, and the small-signal parameters with temperature for the two devices are presented in [15].

In this paper, the performance comparison of MODFET and MESFET is performed to demonstrate the potential of the CESS simulator. The dc performance, the electromagnetic-wave propagation effects, and the equivalent-circuit parameters are presented. In dc simulation, the variation of transconductance and cutoff frequency with gate bias are shown for MODFET and MESFET. The internal distributions of potential, electron concentration, and electron energy are also illustrated. The corresponding results are compared for these two devices.

The electromagnetic-wave propagation effects are observed in the two devices. The output voltage wave increases in magnitude as more and more electromagnetic energy moves along the device width. The device performance in terms of output voltage is compared for the two devices using the electromagnetic model as well as the quasi-static model.

The equivalent-circuit parameters are extracted for MODFET and MESFET using a time-domain technique. Several researchers extracted these parameters employing different techniques [16]–[21]. In this paper, both multiple bias and multiple frequency extractions are done utilizing the hydrodynamic model in time domain. The extracted parameters in this technique are capable of taking care of the nonlinear behavior of the high-frequency devices. The intrinsic small-signal parameters are also extracted from the dc analysis. The dependence of equivalent-circuit parameters on frequency and gate bias is observed.

The MODFET's [see Fig. 1(a)] and the MESFET's [see Fig. 1(b)] are field-effect devices. The MODFET uses

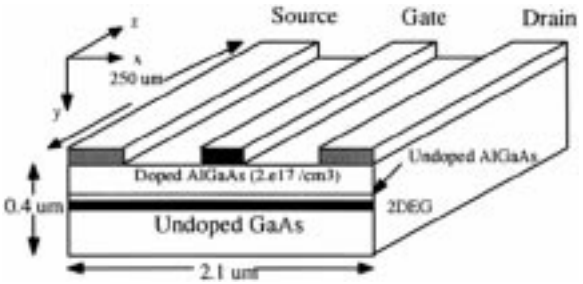

(a)

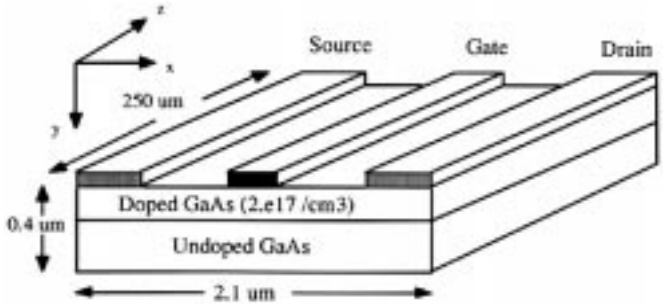

(b)

Fig. 1. The simulated device structures. (a) MODFET. (b) MESFET.

AlGaAs–GaAs heterostructure and have undoped GaAs as an active layer, but the MESFET uses heavily doped GaAs as an active layer. Their very high-speed low-power consumption and relatively simple fabrication technology make them a strong candidate for upper millimeter-wave frequencies [22]. They have excellent power–delay relationship and reduced short channel effects. However, overall MODFET performances are better than those of MESFET's [23].

II. Theory

A. Device Modeling

The CESS simulator is a physically based model, which takes care of nonisothermal transport and nonstationary electron dynamics as well as electromagnetic-wave propagation effects. This model couples the semiconductor model to a 3-D time-domain solution of Maxwell's equations.

The semiconductor model is based on the moments of the Boltzmann's transport equation obtained by integration over the momentum space. The integration results in a strongly coupled highly nonlinear set of partial differential equations called the conservation or hydrodynamic equations [24], [25]. These equations provide a time-dependent self-consistent solution for electron density, electron energy, and electron momentum. The hydrodynamic equations are provided elsewhere [13]. The electronic current density distribution $\boldsymbol{J}$ inside the semiconductor device at any time t is given by

$$\boldsymbol{J}(t) = -q\, n(t)\, \boldsymbol{v}(t). \tag{1}$$

The electromagnetic-wave propagation effects can be completely characterized by solving Maxwell's equations. These equations are first-order linearly coupled differential equations

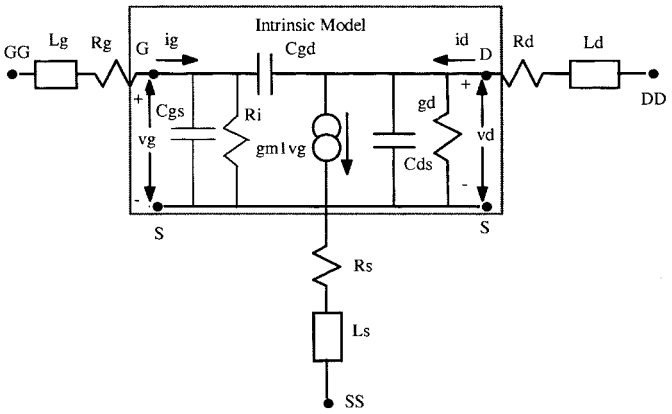

Fig. 2. The generalized equivalent-circuit model for MODFET and MESFET including parasitic elements [26]. Here, $g_{m1} = g_m e^{-j\omega\tau}$.

relating the field vectors, current densities, and charge densities at any point in space at any time. However, they must be supplemented by constitutive relations.

The coupling between the two models is established by using the fields obtained from the solution of Maxwell's equation in the semiconductor model to calculate the current densities inside the device. These current densities are used to update the electric and magnetic fields using Maxwell's equations. The initialization is provided by solving the semiconductor model for the dc charges and currents in response to a specified dc operating point. In this manner, the coupling between the two models results in the overall high-frequency characteristics of the semiconductor devices. The details of the coupling procedure can be found in [13].

B. Equivalent-Circuit Parameters

In this paper, two techniques are used to obtain the equivalent-circuit parameters. One technique is based on the ac analysis, and the other is based on the quasi-static analysis.

1) AC Analysis: The generalized small-signal equivalent-circuit model of MODFET and MESFET is shown in Fig. 2 [26]. The intrinsic part of the device is characterized by the Y admittance matrix [16], [17] obtained from the following equation:

$$\begin{bmatrix} i_{\rm gs} \\ i_{\rm ds} \end{bmatrix} = \begin{bmatrix} Y_{gg} & Y_{\rm gd} \\ Y_{\rm dg} & Y_{\rm dd} \end{bmatrix} \begin{bmatrix} v_{\rm gs} \\ v_{\rm ds} \end{bmatrix}. \tag{2}$$

A sinusoidal voltage of different frequency is applied to the gate and drain of the device separately, and the current and the voltage waveforms are obtained. The admittances are obtained from the magnitude and the relative phase information of these current and voltage waveforms. The equivalent-circuit parameters are extracted from the real and imaginary parts of the admittances. This process is repeated at different frequencies to obtain the frequency dependence of the small-signal parameters.

2) DC Analysis: In dc analysis, the static I–V characteristics are obtained first. The intrinsic small-signal parameters are extracted according to the following basic definitions:

$$\begin{aligned} g_m &= \left|\frac{\partial i_{\rm ds}}{\partial v_{\rm gs}}\right|_{v_{d=\rm const.}} \\ C_{\rm gs} &= \left|\frac{\partial Q_g}{\partial v_{\rm gs}}\right|_{v_{d=\rm const.}} \\ R_i &= \left[{\rm Re}\left(\frac{\partial i_{\rm gs}}{\partial v_{\rm gs}}\right)\right]^{-1}_{v_{d=\rm const.}} \\ g_d &= \left|\frac{\partial i_{\rm ds}}{\partial v_{\rm ds}}\right|_{V_{g=\rm const.}} \\ C_{\rm ds} &= \left|\frac{\partial Q_d}{\partial v_{\rm ds}}\right|_{v_{d=\rm const.}} \\ C_{\rm gd} &= \left|\frac{\partial Q_g}{\partial v_{\rm dg}}\right|_{V_{g=\rm const.}}. \end{aligned} \tag{3, 4}$$

A small perturbation is applied at different bias points and these parameters are obtained.

III. Numerical Techniques

A. Device Simulation

The finite-difference scheme was used in semiconductor device simulations. This scheme lends itself naturally to the simple rectangular geometry generally considered for semiconductor device modeling. In this paper, several finite-difference techniques, such as the upwind and the Lax methods, are used in conjunction with the basic finite-difference formulation to achieve stable and accurate solutions [27]. The hydrodynamic equations are coupled highly nonlinear partial differential equations. The finite-difference scheme decouples these equations. The solution is obtained in a self-consistent evaluation of the three equations in conjunction with Maxwell's equations. The order of the solution goes in the following manner:

1) momentum balance equation is solved;
2) energy balance equation is solved;
3) continuity equation is solved.

The current density distribution is calculated next using (1).

A high-frequency sinusoidal excitation is applied on top of the dc distribution. Maxwell's equations are solved for the updated electric and magnetic fields in response to the sinusoidal excitation and the device current. The time-domain solution of Maxwell's equations is obtained using a 3-D mesh where field components are arranged following Yee's method [28]. Using a first-order differencing, Maxwell's equations can be decoupled over a small time interval Δt. These new fields from Maxwell's equations are used in the semiconductor model for the updated values of the current densities. These current densities are then used in Maxwell's equations in the following time step of the sinusoidal excitation. This simulation process advances in the time domain until some appreciable electromagnetic-wave propagation effects are achieved. The details of the numerical technique can be found in [13].

Higdon's second-order boundary conditions are used to prevent the reflections from the sides, i.e., from the back

TABLE I
DEVICE PARAMETERS USED IN THE SIMULATION

Drain and source contacts	0.46 μm
Gate-source separation	0.4 μm
Gate-drain separation	0.56 μm
Device thickness	0.4 μm
Device width	250 μm
Device length	2.1 μm
Gate length	0.22 μm
Spacer layer thickness	60 A
Active (AlGaAs) layer thickness	0.1 μm
Active (AlGaAs) layer doping	$2x10^{17}$ cm^{-3}
Schottky barrier height	0.8 V
DC gate-source voltage, V_{gso}	-0.5 V
AC gate-source voltage, Δvgs	0.1 and 0.3 V
Operating frequency, f	1 - 120 GHz

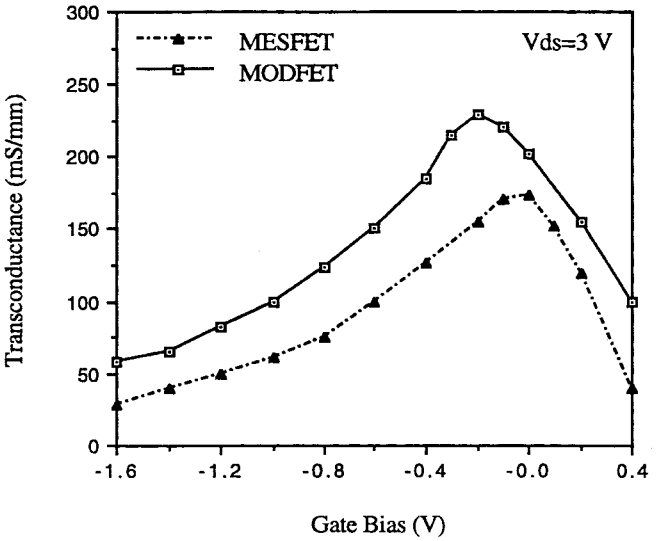

Fig. 4. Comparison of transconductances of MODFET and MESFET structures.

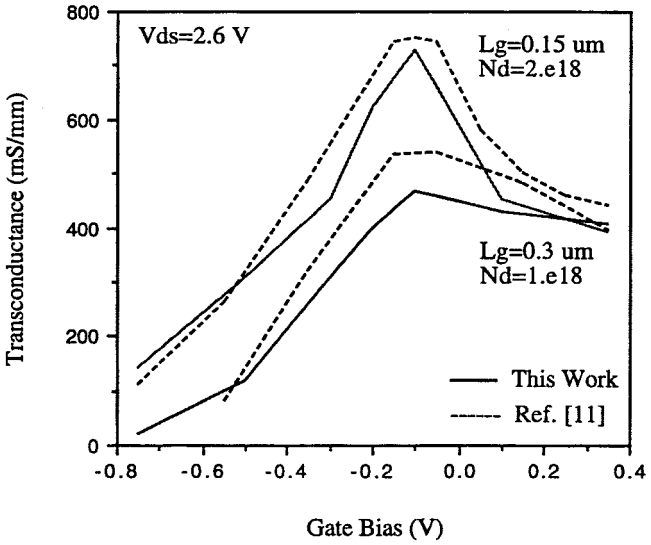

Fig. 3. Comparison of transconductance of MODFET with [11] for different gate lengths.

($z = w$) and from the right and left sides [29]. First-order absorbing boundary conditions are used on the top and bottom, as the field strengths are considerably low at these surfaces. Both explicit and semi-implicit schemes have been incorporated to develop the model. The semi-implicit scheme offers a more stable simulation model. The stability criteria for the semiconductor model and the electromagnetic model provide different time constraints for the simulation. Hence, different time intervals are successfully used for the two models. The $\Delta t_{\text{semiconductor}}$ = ten times of $\Delta t_{\text{electromagnetic}}$. As this technique is computationally intensive, the simulation is performed on a massively parallel (MasPar) machine.

B. Extraction of Small-Signal Parameters

A high-frequency sinusoidal voltage of peak 0.1 V and frequency 10 GHz is applied at the gate for different gate dc biases, with no ac signal at the drain. Then, the waveforms of the gate voltage, gate current, and drain current are obtained according to the simulation model explained in the previous section. This procedure is repeated when the same ac input is applied at the drain for different gate dc biases, with no ac signal at the gate. The waveforms of the drain voltage, gate current, and drain current are similarly obtained. The admittances are calculated according to (2), from the magnitude and the relative phase information of the voltage and current waves.

The intrinsic small-signal parameters are extracted from the admittances. These parameters are then extracted for the frequency range of 20–120 GHz with an interval of 10 GHz. In quasi-static analysis, these parameters are obtained using (3) and (4) by applying a small perturbation at the dc biases. Since this is a quasi-static approach, no frequency dependence can be directly obtained.

IV. RESULTS AND DISCUSSIONS

A. DC Analysis

The simulation parameters of MODFET [see Fig. 1(a)] and MESFET [see Fig. 1(b)] are summarized in Table I. In order to validate the CESS simulator, a MODFET structure similar to Shawki *et al.* [11] is simulated to compare the performances. The transconductances are compared for aspect ratios of 7.5 and 3.75. They exhibit reasonable agreement with each other in Fig. 3.

In Fig. 4, the variation of transconductance g_m with gate bias v_{gs} is shown. The maximum transconductance of 229 mS/mm and 174 mS/mm are obtained for MODFET and MESFET, respectively. A compression in g_m is noticed for both the devices for large positive and negative values of v_{gs}. For large negative v_{gs}, it is due to the electron's injection deep into the GaAs layer and the negligible effect of v_{gs} on those electrons. On the other hand, for MODFET at large positive v_{gs}, this is attributed to the combined effect

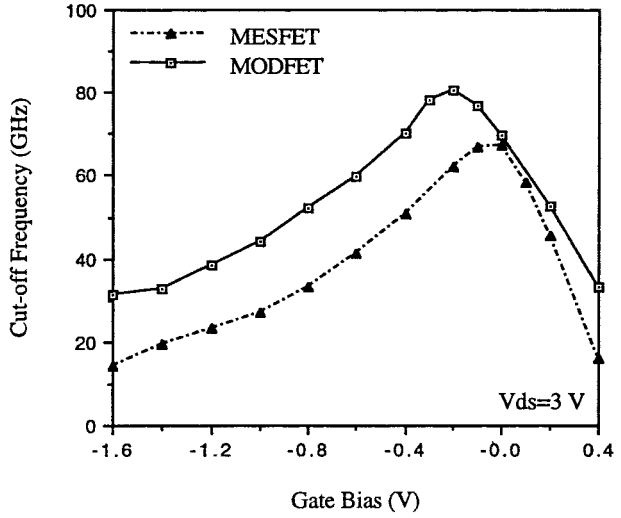

Fig. 5. Comparison of cutoff frequencies of MODFET and MESFET structures.

of the onset of parallel current conduction paths under the gate within the highly doped AlGaAs layer and the complete formation of two-dimensional electron gas (2DEG) which no longer responds to the variations in gate voltages. For MESFET, it is due to the parasitic MESFET effect. The variation of cutoff frequency f_T with gate bias $v_{\rm gs}$ is shown in Fig. 5. The maximum f_T of 81 and 67.5 GHz is obtained for MODFET and MESFET, respectively. The transconductance and the cutoff frequency are higher for MODFET, which support its potential for high-speed operations. The maximum transconductance and the maximum cutoff frequency occur for MODFET at higher reverse gate voltage than MESFET, which is expected.

The state of the MODFET and MESFET under dc steady-state conditions are represented by the contour plots for potential, electron density, and electron energy as shown in Figs. 6 and 7, respectively. The devices are biased to $v_{\rm ds} = 4.0$ V and $v_{\rm gs} = -0.5$ V and the dc distributions are obtained by solving the semiconductor model only. Figs. 6(a) and 7(a) show the equipotential lines with steps of 0.5 V. It can be seen that most of the applied voltage is absorbed in the channel near the drain edge of the gate. Figs. 6(b) and 7(b) show the contour plots of the carrier concentration with steps of 2×10^{16} /cm^3. The corresponding energy contour lines are shown in Figs. 6(c) and 7(c) for energies with steps of 0.1 eV. The region between the gate and the drain is of high energy, where the electric field is strong, especially at the drain edge of the gate where the energy exceeds 0.7 eV for MODFET and 0.5 eV for MESFET. The formation of two-dimensional electron gas is evident in MODFET and the electrons get hotter in the case of MODFET as opposed to MESFET.

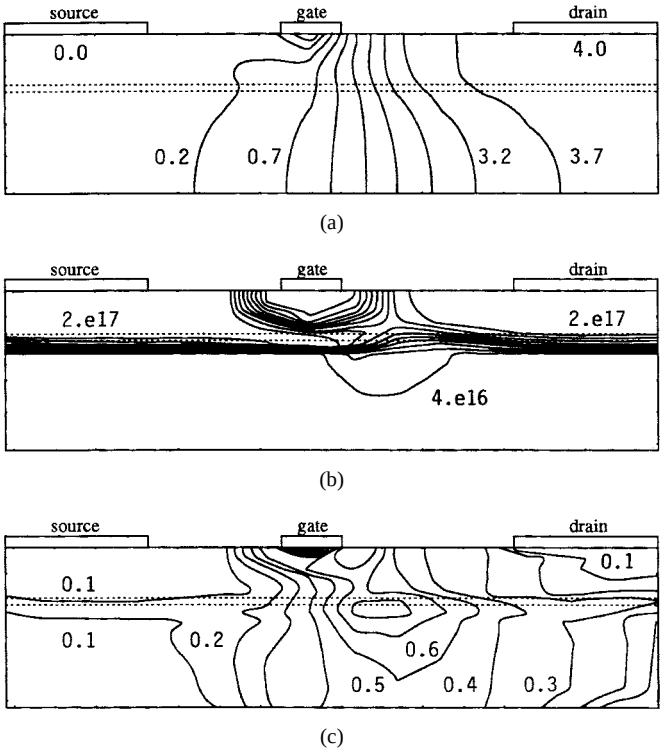

Fig. 6. The contour plots for MODFET. The potential is drawn with steps of 0.5 V, the electron density with steps of 2×10^{16}/cm^3, and the energy with 0.1 eV.

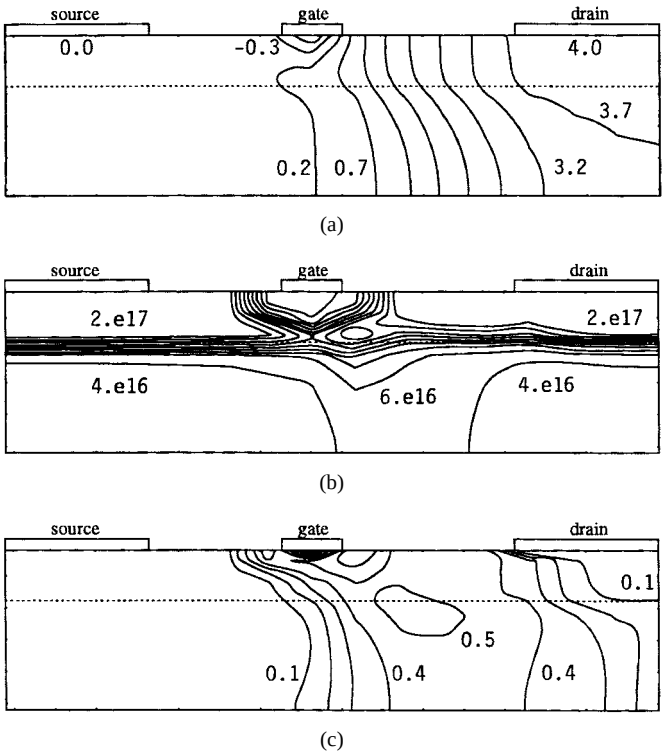

Fig. 7. The contour plots for MESFET. The potential is drawn with steps of 0.5 V, the electron density with steps of 2×10^{16}/cm^3, and the energy with 0.1 eV.

B. Effects of Electromagnetic-Wave Propagation

To demonstrate the electromagnetic-wave propagation effects for MODFET and MESFET, a sinusoidal excitation of a peak of 0.1 V and 80-GHz frequency is applied between the gate and the source electrodes. The total gate voltage becomes

$$v_{\rm gs}(t) = v_{\rm gso} + \Delta v_{\rm gs} \sin(\omega t) \tag{5}$$

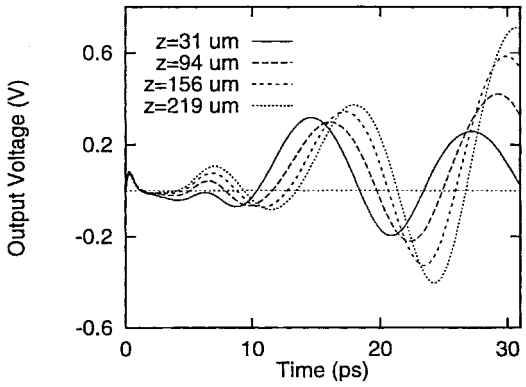

Fig. 8. The electromagnetic-wave propagation effects on output voltages of MODFET for different device widths.

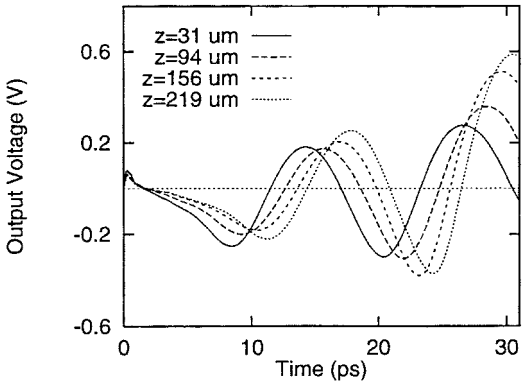

Fig. 9. The electromagnetic-wave propagation effects on output voltages of MESFET for different device widths.

where $v_{\rm gso}$ and $\Delta v_{\rm gs}$ are the dc and the peak ac voltages, respectively. The excitation is applied as a plane source at $z = 0$, as shown in Fig. 1. The CESS model is then solved for a few RF cycles, several tens of picoseconds, to avoid the effects of the transients on the ac solution. The output is obtained across the drain and source at several points along the device width in the z-direction.

The effects of the device wave interaction on the two devices can be represented by the output waveforms for different device widths in the z-direction. The output voltage wave, as shown in Figs. 8 and 9, takes a finite time to respond to the input voltage wave. This delay is due to the finite device-switching time. Early in the simulation, the electronic effect is not present and the wave amplitude decreases along the device width. Later, as more and more electromagnetic energy is propagated along the device width, the wave energy builds up, and the wave amplitude increases. The higher amplitude of the output voltage wave is observed for MODFET than MESFET, which is expected. These figures clearly demonstrate the direct relationship between the device gain characteristics and the electromagnetic-wave propagation.

The effect of using the electromagnetic model in device simulation is demonstrated in Fig. 10. MODFET and MESFET are simulated using the quasi-static model as well as the CESS simulator. In the quasi-static model, Poisson's equation is solved to get the electric fields. In the electromagnetic model, Maxwell's equations are solved to obtain the electric and

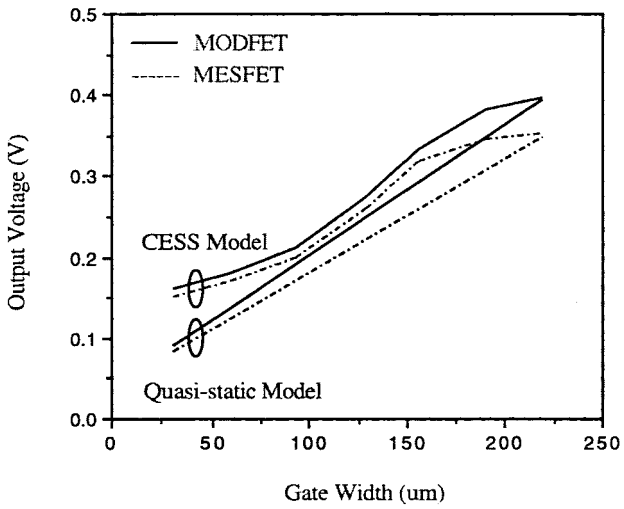

Fig. 10. The comparison of output voltage variations with device width obtained from the CESS model and the quasi-static model for MODFET and MESFET.

magnetic fields. In Fig. 10, the output voltage wave is shown for different device widths using these two models. MODFET has higher output voltage than MESFET, which is evident from both the models. The output voltage wave monotonously increases along the device width in the quasi-static model. On the other hand, in the electromagnetic model, the output voltage wave nonlinearly increases with the device width. This phenomenon is expected due to the device–electromagnetic-wave interaction. The exchange of energy between the electrons and the electromagnetic wave takes place along the device width. This behavior is absent when the output is obtained from the quasi-static analysis. Thus, the CESS model provides the opportunity to choose the optimized device width for maximum output voltage. This figure strongly supports the use of the electromagnetic model for device simulation at high frequencies.

In Fig. 11, the output voltage is shown for different frequency using the quasi-static as well as the electromagnetic model. The device width is 200 μm. As expected, the output voltage is higher for MODFET than MESFET in both the models. The output voltage decreases with frequency for the two devices. However, the differences in output voltage at high frequencies, obtained from these two models, demonstrate the potential of using the electromagnetic model in device simulation to get the correct device response.

The electromagnetic-wave propagation effect is validated by simulating a MESFET structure similar to [30]. The MESFET has the following dimensions. The gate–source spacing = 1.5 μm, gate–drain spacing = 1.5 μm, gate length = 0.5 μm, gatewidth = 1 mm, active layer thickness = 0.2 μm, active layer doping = $1 \times 10^{17}/\text{cm}^3$. Two input voltages were used in the simulation: 0.1 and 0.3 V. Fig. 12 shows the comparison of the gain performances. The results exhibit the same trend; however, as expected, there are quantitative differences. In this paper, the CESS simulator was used, which gives the exact device behavior. In [30], the equivalent-circuit approach was utilized. The difference in results is due to the use of the full electromagnetic model and also retaining

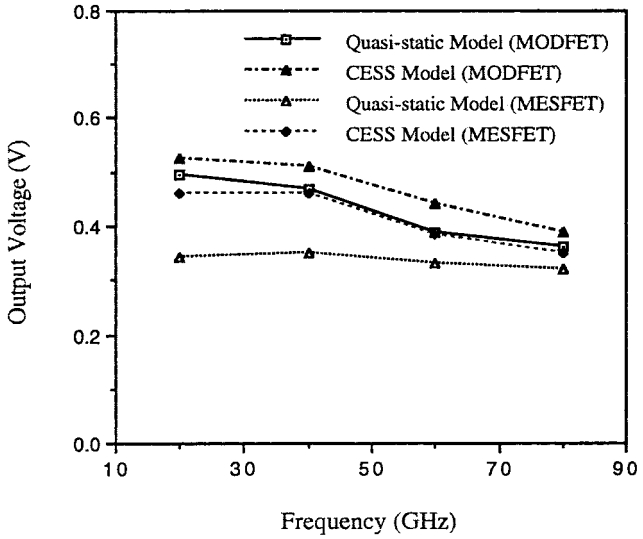

Fig. 11. The comparison of the output voltage with different frequency obtained from the CESS model and the quasi-static model for MODFET and MESFET.

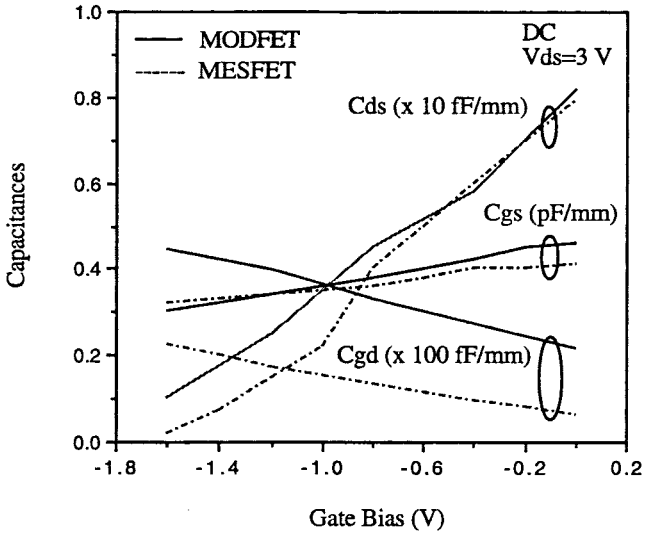

Fig. 13. Variations of gate–source capacitance $C_{\rm gs}$, feedback capacitance $C_{\rm gd}$, and drain–source capacitance $C_{\rm ds}$ with gate bias for MODFET and MESFET using quasi-static approach.

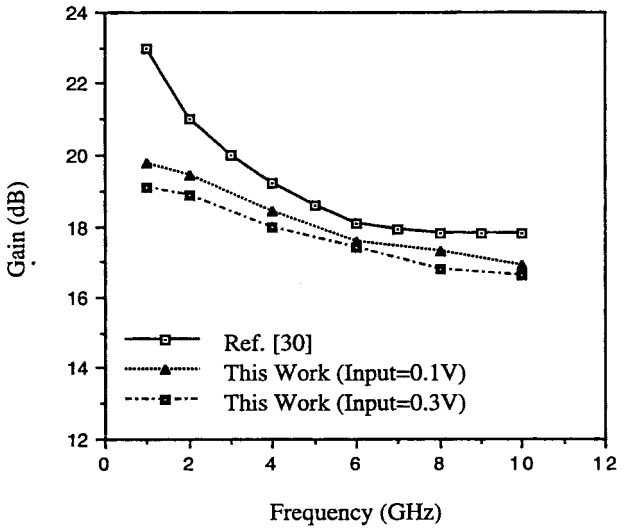

Fig. 12. The comparison of gain characteristics of MESFET with that of [30]. The gain characteristics for large-signal operation are also shown for an input voltage of 0.3 V.

the large-signal aspects in the CESS model, while the data for [30] is strictly a small-signal approach. To demonstrate the large-signal potential of the CESS simulator, the gain was recalculated for an input signal of 0.3 V. As shown in Fig. 12, the gain becomes lower as the amplitude increases, which is expected. The strength of this approach is not in simply confirming that larger amplitudes reduce the gain, but in estimating the reduction directly, using the physical model. Moreover, the harmonics generated by the device nonlinearity can be analyzed by taking the Fourier transform of the output signal. To the best of our knowledge, the CESS model is the only direct approach that can perform this study.

C. Equivalent-Circuit Model

The generalized equivalent-circuit model is already shown in Fig. 2 for MODFET and MESFET. The intrinsic small-signal parameters (inside the dashed rectangle) are extracted using the ac dynamic approach, as well as using the quasi-static approach.

The equivalent-circuit parameters extracted from the quasi-static approach are reported first. The variations of gate–source capacitance $C_{\rm gs}$, feedback capacitance $C_{\rm gd}$, and drain–source capacitance $C_{\rm ds}$ with gate bias $v_{\rm gs}$ are shown for MODFET and MESFET in Fig. 13. The magnitude of $C_{\rm gs}$ increases as $v_{\rm gs}$ becomes more positive due to the accumulation of electrons in the undepleted AlGaAs (doped GaAs for MESFET) region close to the gate electrode. The observed increase in $C_{\rm gd}$ with large negative $v_{\rm gs}$ values results from the side broadening of the depletion zone so that its edge close to the drain will be more sensitive to the variations in $v_{\rm ds}$. On the other hand, for large positive values of $v_{\rm gs}$, the right-edge of the gate depletion zone moves toward the gate and is hardly affected by the change in $v_{\rm ds}$. The value of $C_{\rm ds}$ increases with gate bias. The magnitude of $C_{\rm ds}$ is relatively small because enough substrate region was not simulated due to computational limitations. The difference in parametric values for the two devices are as expected.

The variations for the two devices of some of the equivalent-circuit parameters at different frequencies are shown in Figs. 14–16. The dependence of $C_{\rm gs}$ on frequency for different $v_{\rm gs}$ is compared in Fig. 14 for MODFET and MESFET. The magnitude of $C_{\rm gs}$ decreases as the frequency increases. The variation is more prominent in MODFET than MESFET. At high frequencies, the displacement current from gate-to-drain contact becomes significant. As a result, the impedance between the gate and drain contacts decreases. It eventually increases the feedback capacitance $C_{\rm gd}$. Since the total charge stored is a function of the bias point, the increase in $C_{\rm gd}$ must be compensated by a decrease in $C_{\rm gs}$. The dependence of transconductance g_m on frequency is demonstrated in Fig. 15 for MODFET and MESFET. The magnitude of g_m decreases at high frequencies. When the displacement current increases at high frequencies, the fraction of the total current flowing

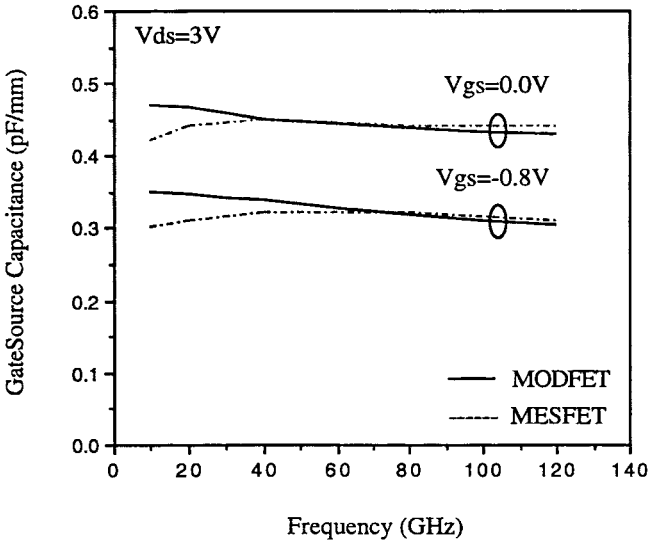

Fig. 14. Variations of gate–source capacitance $C_{\rm gs}$ with frequency for MODFET and MESFET at two gate biases.

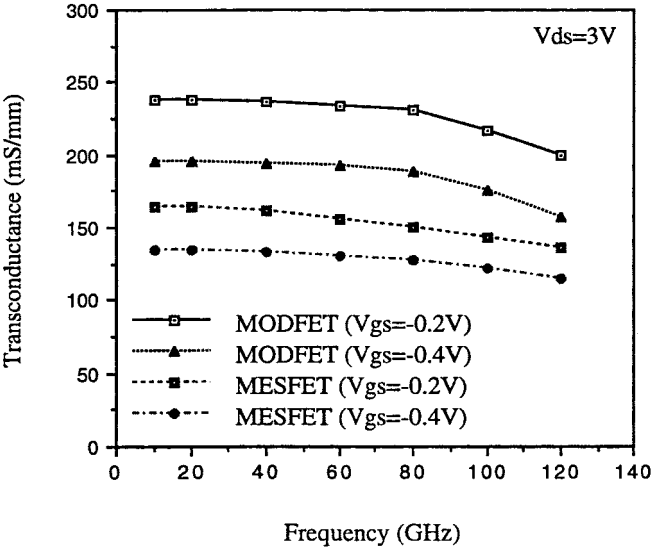

Fig. 15. Dependence of transconductance g_m on frequency for MODFET and MESFET at two gate biases.

through the channel region between the source and the drain decreases, which is reflected as an effective decrease in g_m. The variations of drain–source capacitance $C_{\rm ds}$ with frequency for different $v_{\rm gs}$ are shown in Fig. 16. The magnitude of $C_{\rm ds}$ increases with the increase of frequency.

V. Conclusions

A CESS simulator is demonstrated for the complete analysis of submicrometer semiconductor devices, including the electromagnetic-wave propagation effects. The performance comparison of two important high-frequency devices—MODFET and MESFET—are presented. The results of the simulation provide a number of important findings summarized as follows.

1) The simulation uses the electromagnetic-wave concept to emphasize the better performance of MODFET over MESFET.

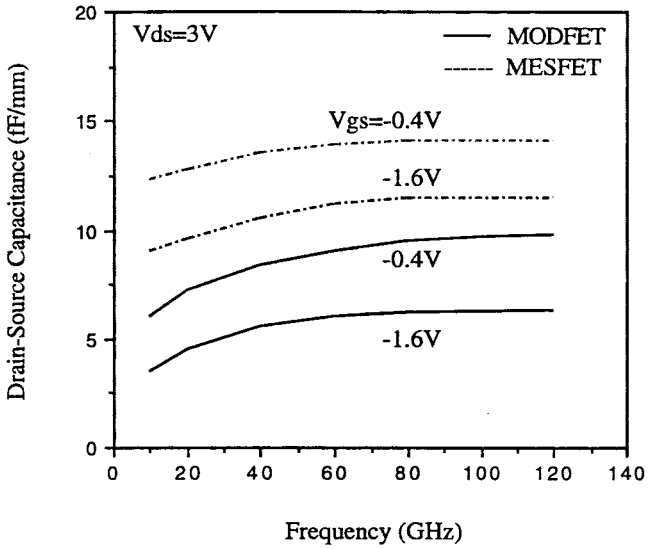

Fig. 16. Variations of drain–source capacitance $C_{\rm ds}$ with frequency for MODFET and MESFET at two gate biases.

2) The simulation confirms that a significant device wave interaction takes place in high-frequency devices.
3) The energy exchange between the electromagnetic wave and the electrons results in an increase in the output-voltage wave amplitude along the device width the electromagnetic model is required in the device simulation at high frequencies.
4) The CESS simulator is capable of handling the large-signal operation successfully.
5) The equivalent-circuit parameters depend on frequency as well as on gate bias.
6) Reasonable agreement is achieved in comparison with published results. This fact validates the accuracy of the CESS simulator.

The CESS model used in this paper has interesting contributions toward the complete characterization of microwave and millimeter-wave devices. The immediate application is the optimization of the device geometry and the parameters. The problems of electromagnetic coupling, discontinuities, and parasitic elements resulting from distribution pads can be studied. The complete characterization of a microwave amplifier with input and output matching networks were developed using the CESS simulator [12].

References

[1] M. S. Shur, "Analytical model of GaAs MESFET's," *IEEE Trans. Electron Devices*, vol. ED-25, pp. 612–618, June 1978.
[2] B. Carnez, A. Cappy, A. Kaszynski, E. Constant, and G. Salmer, "Modeling of a sub-micrometer gate field-effect transistors including effects of nonstationary electron dynamics," *J. Appl. Phys.*, vol. 51, no. 1, pp. 784–790, Jan. 1980.
[3] D. Delagebeaudeuf and N. T. Linh, "Metal-(n) AlGaAs–GaAs two-dimensional electron gas FET," *IEEE Trans. Electron Devices*, vol. ED-29, pp. 955–960, June 1982.
[4] K. Lee, M. S. Shur, T. J. Drummond, and H. Morkoc, "Current–voltage and capacitance–voltage characteristics of modulation doped field-effect transistors," *IEEE Trans. Electron Devices*, vol. ED-30, pp. 207–212, Mar. 1983.
[5] C. M. Snowden, M. J. Howes, and D. V. Morgan, "Large-signal modeling of GaAs MESFET operation," *IEEE Trans. Electron Devices*, vol. ED-30, pp. 1817–1824, Dec. 1983.

[6] M. H. Weiler and Y. Ayasli, "DC and microwave models for $Al_x Ga_{1-x}As$/GaAs high electron mobility transistors," *IEEE Trans. Electron Devices*, vol. ED-31, pp. 1854–1861, Dec. 1984.
[7] C. M. Snowden and D. Loret, "Two-dimensional hot-electron models for short-gate-length GaAs MESFET's," *IEEE Trans. Electron Devices*, vol. ED-34, pp. 212–223, Feb. 1987.
[8] P. Roblin, S. Kang, A. Ketterson, and H. Morkoc, "Analysis of MODFET microwave characteristics," *IEEE Trans. Electron Devices*, vol. ED-34, pp. 1919–1928, Sept. 1987.
[9] S. M. El-Ghazaly and T. Itoh, "Two-dimensional numerical simulation of short-gate-length GaAs MESFET's and application to the traveling Gunn domain phenomenon," *Int. J. Numer. Modeling*, vol. 1, pp. 19–30, Jan. 1988.
[10] Y. K. Feng and A. Hintz, "Simulation of sub-micrometer GaAs MESFET's using a full dynamic transport model," *IEEE Trans. Electron Devices*, vol. 35, pp. 1419–1431, Sept. 1988.
[11] T. Shawki, G. Salmer, and O. El-Sayed, "MODFET 2-D hydrodynamic energy modeling: Optimization of subquarter-micron gate structure," *IEEE Trans. Electron Devices*, vol. 37, pp. 21–30, Jan. 1990.
[12] S. M. S. Imtiaz and S. M. El-Ghazaly, "Global modeling of millimeter-wave circuits: Electromagnetic simulation of amplifiers," *IEEE Trans. Microwave Theory Tech.*, vol. 45, pp. 2208–2216, Dec. 1997.
[13] M. A. Alsunaidi, S. M. S. Imtiaz, and S. M. El-Ghazaly, "Electromagnetic wave effects on microwave transistors using a full-wave time domain model," *IEEE Trans. Microwave Theory Tech.*, vol. 44, pp. 799–808, June 1996.
[14] M. B. Das, "Millimeter-wave performance of ultrasubmicrometer-gate field-effect transistor: A comparison of MODFET, MESFET, and PBT structures," *IEEE Trans. Electron Devices*, vol. ED-34, pp. 1429–1440, July 1987.
[15] Y. Gobert and G. Salmer, "Comparative behavior and performance of MESFET and HEMT as a function of temperature," *IEEE Trans. Electron Devices*, vol. ED-41, pp. 299–305, Mar. 1994.
[16] G. Dambrine, A. Cappy, F. Heliodore, and E. Playez, "A new method for determining the FET small-signal equivalent circuit," *IEEE Trans. Microwave Theory Tech.*, vol. 36, pp. 1151–1159, July 1988.
[17] M. Berroth and R. Bosch, "High-frequency equivalent circuit of GaAs FET's for large signal applications," *IEEE Trans. Microwave Theory Tech.*, vol. 39, pp. 224–229, Feb. 1991.
[18] H.-O. Vickes, "Determination of intrinsic FET parameters using circuit partitioning approach," *IEEE Trans. Microwave Theory Tech.*, vol. 39, pp. 363–366, Feb. 1991.
[19] K. Shirakawa, H. Oikawa, T. Shimura, Y. Kawasaki, Y. Ohashi, T. Saito, and Y. Daido, "An approach to determining an equivalent circuit for HEMT's," *IEEE Trans. Microwave Theory Tech.*, vol. 43, pp. 499–503, Mar. 1995.
[20] T. Gonzalez and D. Pardo, "Monte Carlo determination of the intrinsic small-signal equivalent circuit of MESFET's," *IEEE Trans. Electron Devices*, vol. 42, pp. 605–611, Apr. 1995.
[21] R. Singh and C. M. Snowden, "Small-signal characterization of microwave and millimeter-wave HEMT's based on physical model," *IEEE Trans. Microwave Theory Tech.*, vol. 44, pp. 114–121, Jan. 1996.
[22] H. Daembkes, *Modulation-Doped Field-Effect Transistor Principles, Design, and Technology*. Piscataway, NJ: IEEE Press, 1990.
[23] H. Morkoc and P. M. Solomon, "The HEMT: A superfast transistor," *IEEE Spectrum Mag.*, vol. 21, pp. 28–35, Feb. 1984.
[24] K. Blotekjaer, "Transport equations for electrons in two-valley semiconductors," *IEEE Trans. Electron Devices*, vol. ED-17, pp. 38–47, Jan. 1970.
[25] M. Shur, "Influence of nonuniform field distribution on frequency limits of GaAs field-effect transistors," *Electron. Lett.*, vol. 12, pp. 615–616, 1976.
[26] J. M. Golio, *Microwave MESFET's and HEMT's*. Norwood, MA: Artech House, 1991.
[27] A. R. Mitchell and D. F. Griffiths, *The Finite Difference Method in Partial Differential Equations*. New York: Wiley, 1987.
[28] K. S. Yee, " Numerical solution of initial boundary value problems involving Maxwell's equations in isotropic media," *IEEE Trans. Antennas Propagat.*, vol. AP-14, pp. 302–307, Jan. 1966.
[29] R. L. Higdon, "Numerical absorbing boundary conditions for the wave equation," *Math. Comp.*, vol. 49, pp. 65–91, July 1987.
[30] M. S. Hakim and S. M. El-Ghazaly, "Analysis of wave propagation effects on microwave field-effect transistors," in *IEEE MTT-S Dig.*, Atlanta, GA, 1993, pp. 1303–1306.

S. M. Sohel Imtiaz (S'94–M'96) was born in Dhaka, Bangladesh, in 1966. He received the B.S. and M.S. degrees in electrical engineering from Bangladesh University of Engineering and Technology (BUET), Dhaka, Bangladesh, in 1988 and 1990, respectively, and the Ph.D. degree in electrical engineering from Arizona State University (ASU), Tempe, in 1997.

From 1989 to 1991, he was a Lecturer in the Department of Electrical and Electronic Engineering, Bangladesh University of Engineering and Technology. From 1993 to 1997, he was a Teaching/Research Associate in the Department of Electrical Engineering, ASU. In 1997, he joined Micro Linear Corporation, San Jose, CA, as a Senior Device Engineer. His research interests include the modeling and simulation of microwave and millimeter-wave semiconductor devices and circuits, device wave interactions, numerical techniques, extraction of equivalent-circuit parameters of semiconductor devices, and the design, modeling, and simulation of microwave amplifiers.

Dr. Imtiaz is a member of the IEEE Microwave Theory and Techniques, Electron Devices, and Solid-State Circuits Societies.

Samir M. El-Ghazaly (S'84–M'86–SM'91) received the Ph.D. degree in electrical engineering, from the University of Texas at Austin, in 1988.

In 1988, he joined Arizona State University, Tempe, as an Assistant Professor, and became Professor in 1998. He has worked at several universities and research centers, including the College of Engineering, Cairo University, Cairo, Egypt, as a Teaching Assistant and Assistant Lecturer, the Centre Hyperfrequences et Semiconducteurs, Université de Lille I, France, where he worked on the simulation of submicron-gate MESFET's, University of Ottawa, Ottawa, Ont., Canada, where he worked on the analysis of E-plane circuits, the University of Texas at Austin, first as a Research Assistant and then as a Post-Doctoral Fellow, Jet Propulsion Laboratory, NASA, Pasadena, CA, where he was a Summer Faculty Research Fellow working on millimeter-wave mixers, CST-Motorola, Inc., while on sabbatical leave from ASU, working on modeling semiconductor devices for RF applications, and IEMN, Université de Lille, France, as a Visiting Professor. His research interests include microwave and millimeter-wave semiconductor devices and passive circuits, semiconductor device simulations, ultra-short pulse propagation, linear and nonlinear modeling of superconductor microwave lines, wave-device interactions, electromagnetics, and numerical techniques applied to monolithic microwave integrated circuits. He is the secretary of the U.S. National Committee of URSI, Commission A.

Dr. El-Ghazaly is a member of Tau Beta Pi, Sigma Xi, and Eta Kappa Nu, and an elected member of Commissions A and D of URSI. Since 1991, he has been a member of the Technical Program Committee for the IEEE International Microwave Symposium and is on the editorial board of the IEEE TRANSACTIONS ON MICROWAVE THEORY AND TECHNIQUES. He was the chairman of the IEEE-Waves and Devices Group, Phoenix Section. Since 1992, he has been the Chapter Funding Coordinator for IEEE Microwave Theory and Techniques Society (MTT-S). He is currently the chairman of the Chapter Activities Committee of the IEEE MTT-S.